Fluid Dynamics & Materials Processing
DOI:10.32604/fdmp.2020.09673
Article

Determination of the Circulation for a Large-Scale Wind Turbine Blade Using Computational Fluid Dynamics

Hao Cheng, Guangsheng Du*, Meng Zhang, Kun Wang and Wenbin Bai

School of Energy and Power Engineering, Shandong University, Jinan, 250061, China
*Corresponding Author: Guangsheng Du. Email: du@sdu.edu.cn
Received: 14 January 2020; Accepted: 28 April 2020

Abstract: The determination of the circulation for wind turbine blades is an important problem in engineering. In the present study, we develop a specific approach to evaluate the integral that represents mathematically the circulation. First the potentialities of the method are assessed using a two-dimensional NACA64_A17 airfoil as a testbed and evaluating the influence of different integration paths and angles of attack on the circulation value. Then the method is applied to blades with different relative heights in order to provide useful reference data to be used for the optimization and reverse design of wind turbine blades. As shown by the results, the integral value changes with the integral path, and an "optimal circle radius" exists. We calibrate the integral value by comparing its value with the lift formula. In this was we succeed in showing that there is a certain error when the radius is too small. However, the error can increase rapidly when the radius is too large. When the radius of the circle is 1–6 times the chord length, the error of all integral values is less than 5%. The optimal radius varies with the angle of attack.

Keywords: Airfoil; lift; wind turbine; circulation distribution

1 Introduction

With the aggravation of the world energy economic crisis, countries all over the world have formulated energy transformation strategies. Wind power which is a kind of clean and renewable energy has become a major development target of all countries [1].

With the development of computer technology and the improvement of three-dimensional turbulence technology, computational fluid dynamics (CFD) plays an increasingly important role in the study of complex flow field characteristics. Blade is the key part of energy conversion of wind turbine, thus the aerodynamic design and structural design of wind turbine blades are more and more important [2]. Researchers have done a lot of research on the aerodynamic characteristics and structural optimization design of wind turbine: Benjanirat analyzed the results of aerodynamic simulation of wind turbine based on Baldwin-Lomax turbulence model. Spalart-Allmaras turbulence model and K-ε turbulence model were used respectively, and were compared the impact of near wall treatment on the simulation results. The analysis showed that K-ε turbulence model combined with the comparison near wall treatment could get better results [3]. Kenji et al. [4] used DSD/SST method to simulate the aerodynamic characteristics of

This work is licensed under a Creative Commons Attribution 4.0 International License, which permits unrestricted use, distribution, and reproduction in any medium, provided the original work is properly cited.

wind turbine, and pointed out that the torque calculation needed a very fine numerical simulation method in the case of large Reynolds number and rotating turbulence. Scholars had also done a lot of work on the aerodynamic characteristics of rotating machinery. Zhang et al. [5] conducted the aerodynamic characteristics of k-ω turbulence model and SST k-ω turbulence model respectively. He found that SST k-ω turbulence model had better simulation effect and put forward methods and suggestions to modify the aerodynamic shape of blades. Tian et al. [6] optimized the geometrical parameters of the impeller based on the three-level approach relying on the orthogonal test method. Calculated the head and efficiency under the rated flow rate of different schemes, processed with the method of range analysis to obtain an optimized model. Yang et al. [7] established the dynamic model of wind speed and its spatiotemporal distribution model about the swept surface of wind turbine by comprehensively considering the fluctuating wind speed model of wind shear tower shadow effect. They accurately simulating the speed time variation relationship of each point on the swept surface of wind turbine. Chen et al. [8] studied the dynamics of dispersed bubbles in a centrifugal separator to improve the system efficiency. The kinematic behavior of bubbles is simulated in detail by using discrete phase numerical method. Kriraa et al. [9] studied the natural convection in a vertical convergent channel with a circular block to improve the performance of a wind turbine. Correlated the Nusselt number and the mass flow rate with Rayleigh number. Frulla et al. [10] used the MRF (Moving Reference Frame) technique to simulate the relative rotational motion between the fluid and the wind turbine. The production methods suitable for composite components are critically discussed. Researchers have done a lot of researches on blades and wings optimization design. Kim et al. [11] used the response surface method to design the plane shape and airfoil in an integrated aerodynamic/structural way. Shi et al. [12] optimized the structure size of M6 wing by the response surface method. Liem et al. [13] took the voyage as the optimization objective and built a multidisciplinary optimization platform to carry out multi-point optimization of wing aerodynamic structure for civil airliner. Jiang et al. [14] obtained the geometric twist wing based on the reverse design of the drag reduction of the target circulation distribution and simulated the optimization results by the method of program prediction and numerical simulation. Qiao et al. [15] improved the aerodynamic characteristics of the wind wing with blunt trailing edge. The aerodynamic characteristics of the wind wing with blunt trailing edge were improved and the strength of the detached vortex in the wake area was weakened through the circulation control of the blunt trailing edge wing type. However, there is no in-depth study on the distribution of aerodynamic and circulation characteristics of airfoil, and relevant aerodynamic design laws are not summarized.

In this paper, the optimal path for NACA64_A17 airfoil circulation integral path is presented. The calculation domain is calculated based on Reynolds Average Navier-Stokes turbulence model, which set the integral path and write a program to calculate the circulation. The change of integral value with integral path and angle of attack is studied. Based on the research, the circulation distribution of wind turbine blades under different conditions is analyzed.

2 Methods and Models

2.1 Control Equation

The fluid continuity equation and RANS equation are as follows:

$$\begin{aligned} &\frac{\partial \rho}{\partial t}+\frac{\partial}{\partial x_i}(\rho u_i)=0 \\ &\frac{\partial}{\partial t}(\rho u_i)+\frac{\partial}{\partial x_i}(\rho u_i u_j)=-\frac{\partial p}{\partial x_i}+\frac{\partial}{\partial x_i}[\mu(\frac{\partial u_i}{\partial u_j}+\frac{\partial u_j}{\partial u_i}-\frac{2}{3}\delta_{ij}\frac{\partial u_l}{\partial x_l})]+\frac{\partial}{\partial x_j}(-\rho\overline{u_i' u_j'}) \end{aligned} \tag{1}$$

where u_i and u_j are the time average of wind speed; u_i', u_j' are velocity pulsation; ρ is the density; μ is the viscosity coefficient of the fluid; p is the pressure. For two-dimensional problem, $i = 1, 2$; Three dimensional problem, $i = 1, 2, 3$.

Because the wind turbine impeller is a three-dimensional rotating symmetrical structure, the governing equation is transformed to a rotating coordinate system. The relation between the absolute velocity V describing the velocity field in the static coordinate system and the relative velocity V_r describing the velocity field in the rotating coordinate system is as follows:

$$V_r = V - \Omega \times r \tag{2}$$

where Ω is the angular velocity vector, $\boldsymbol{r}$ is the position vector in the rotating coordinate system.

Continuity equation:

$$\nabla \cdot V = 0 \tag{3}$$

Momentum equation:

$$\frac{\delta V}{\delta t} + \nabla \cdot (V_r V) + \boldsymbol{\Omega} \times V = -\nabla p + \nabla \cdot \boldsymbol{\tau} \tag{4}$$

where μ_t is the coefficient of viscosity of vortex of constant.

In this paper, SST k-ω turbulence model is used to simulate the flow of airfoils and wind turbines by the finite volume method of central difference scheme. It has certain advantages in calculation accuracy and convergence speed in the numerical simulation of circulation control and finite volume method based on the central difference scheme [16,17].

2.2 SST k-ω Turbulence Model

For CFD analysis of aerodynamic performance of airfoils, SST k-ω model is one of the commonly used turbulence models. It is a mixture of k-ω and k-ε models so that the turbulence model has both the reliability of k-ε model to calculate the viscous flow in the near wall area and the accuracy of model to calculate the free flow in the far field.

$$\begin{aligned}
&\frac{\partial}{\partial t}(\rho k) + \frac{\partial}{\partial x_i}(\rho k u_i) = \frac{\partial}{\partial x_j}(\Gamma_k \frac{\partial k}{\partial x_j}) + G_k - Y_k \\
&\frac{\partial}{\partial t}(\rho \omega) + \frac{\delta}{\delta x_i}(\rho \omega u_i) = \frac{\partial}{\delta x_j}(\Gamma_\omega \frac{\partial \omega}{\Delta \partial x_j}) + G_\omega - Y_\omega + D_\omega \\
&\Gamma_k = \mu + \frac{\mu_t}{\sigma_k} \\
&\Gamma_\omega = \mu + \frac{\mu_t}{\sigma_\omega} \\
&\mu_t = \frac{\rho k}{\omega} \alpha^*
\end{aligned} \tag{5}$$

where Γ_k and Γ_ω are the diffusion coefficient, μ_t is the eddy viscosity coefficient, G_k and G_ω are turbulent generation term, Y_k and Y_ω are the turbulent dissipation, α^* is the low Reynolds number correction coefficient, σ_k and σ_ω are the turbulent Prandtl numbers for k and ω, D_ω is the diffusion term.

2.3 The Calculation Method of Circulation

For the flow field of a closed curve, Circulation is defined as the line integral of a velocity vector along the curve:

$$\Gamma = \oint \boldsymbol{v} \cdot \boldsymbol{ds} = \oint (v_x dx + v_y dy + v_z dz) \tag{6}$$

where Γ is the circulation. The integral formula can be used to integrate the data approximately by trapezoidal discrete method and the calculation formula of circulation of the two-dimensional airfoil can be written as:

$$\Gamma = \sum_{i=1}^{n-1} \frac{v_{i+1} v_i}{2} \Delta s_i = \sum_{i=1}^{n-1} [\frac{v_{x_{i+1}} + v_{x_i}}{2} \cdot (x_{i+1} - x_i) + \frac{v_{y_{i+1}} + v_{y_i}}{2} \cdot (y_{i+1} - y_i)] \tag{7}$$

where n is the number of discrete points, and the larger the value of n is, the more accurate the calculation is. 200 points are selected in this paper, and the integration direction is counterclockwise. The program of calculation formula of circulation is written by the MATLB compiler. The selection method of the integral path is as follows: the aerodynamic center of the airfoil is taken as the center of circle which is selected as the variable. As shown in Fig. 1, and the minimum radius is the chord length of the airfoil.

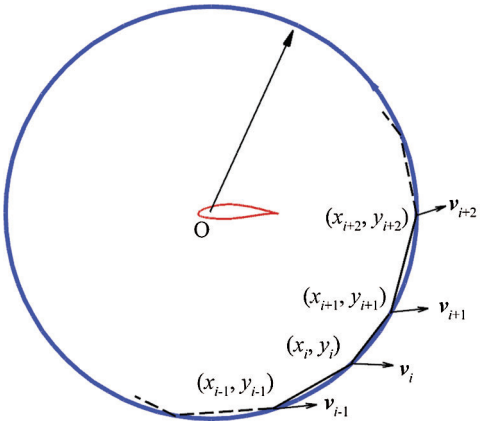

Figure 1: Integral path

According to the Kutta-Joukowski theorem, for steady, ideal and incompressible flows, lift of airfoil is defined as follows under the influence of forces:

$$L = \rho v |\Gamma| \tag{8}$$

where L is the lift force. This formula can be used to deduce the circulation and take it as the reference value. The integral values under different paths are compared with the reference values.

3 Calculation Model and Verification

3.1 Calculation Model

In order to study the size of circle radius, Fluent 6.3 simulation software is used to study the NACA64_A17 two-dimensional airfoil. It is a general purpose CFD package designed to simulate complex flows from incompressible to highly compressible ranges. Fluent uses an element-based finite volume method, which first involves discretizing the spatial domain using a mesh. The mesh is used to

construct finite volumes, which are used to conserve relevant quantities such as mass, momentum, and energy. The Fig. 2 below shows a typical two-dimensional mesh. All solution variables and fluid properties are stored at the nodes (mesh vertices). A control volume (the shaded area) is constructed around each mesh node using the median dual (defined by lines joining the centers of the edges and element centers surrounding the node). To illustrate the finite volume methodology, consider the conservation equations for mass, momentum, and a passive scalar, these equations are integrated over each control volume, and Gauss' Divergence Theorem is applied to convert volume integrals involving divergence and gradient operators to surface integrals. If control volumes do not deform in time, then the time derivatives can be moved outside of the volume integrals and the integrated equations become:

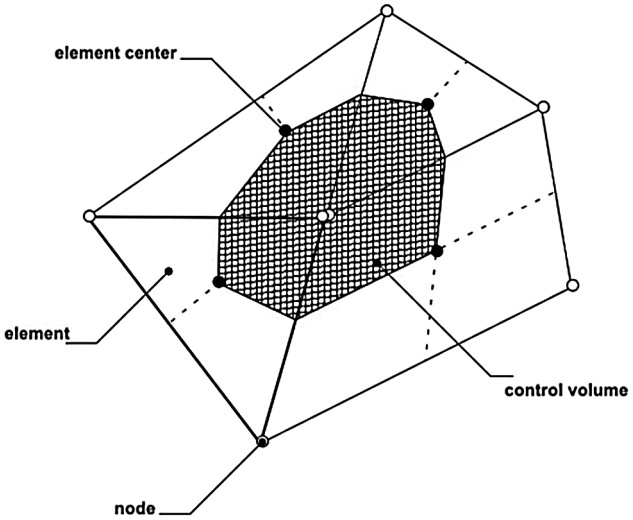

Figure 2: Two-dimensional mesh

$$\frac{d}{dt}\int_V \rho dV + \int_S \rho v_j dn_j = 0$$
$$\frac{d}{dt}\int_V \rho \boldsymbol{U}_i dV + \int_S \rho \boldsymbol{U}_j \boldsymbol{U}_i dn_j = -\int_S P dn_j + \int_S \int_S \mu_{eff}\left(\frac{\partial \boldsymbol{U}_i}{\partial \boldsymbol{x}_j} + \frac{\partial \boldsymbol{U}_j}{\partial \boldsymbol{x}_i}\right) dn_j + \int_V S_{U_i} dV \tag{9}$$
$$\frac{d}{dt}\int_V \rho \varphi dV + \int_S \rho \boldsymbol{U}_j \varphi dn_j = \int_S \Gamma_{eff}\left(\frac{\partial \varphi}{\partial \boldsymbol{x}_j}\right) dn_j + \int_V S_\varphi dV$$

where V and S respectively denote volume and surface regions of integration, and dn_j are the differential Cartesian components of the outward normal surface vector. The volume integrals represent source or accumulation terms, and the surface integrals represent the summation of the fluxes. Due to the adoption of various solving methods and multi-grid accelerating convergence technology, fluent can achieve the best convergence speed and solution accuracy. Flexible unstructured grid, solution-based adaptive grid technology and mature physical model make fluent widely used in conversion and turbulence, heat transfer and phase transition, chemical reaction and combustion, multiphase flow, rotating machinery, dynamic/deformation grid, noise, material processing, fuel cell, etc.

Airfoil parameters include: the chord length of airfoil is 2 m, NACA64 airfoil with an aspect ratio of 17, the position of maximum thickness is 0.74 m and the relative curvature is 3%. The incompressible flow is adopted. In order to reduce the numerical error, a larger calculation domain is taken. The front part of the

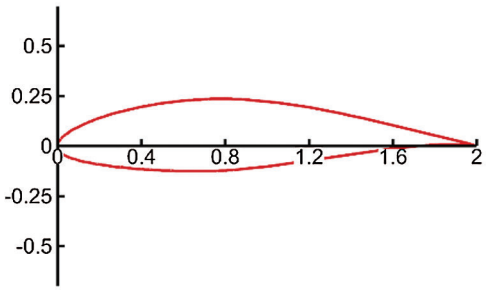

Figure 3: Airfoil

computational domain is the semicircle entrance with 30 times chord length and the back region of the model is a square with a length of 60 times the chord length. The airfoil diagram is shown in Fig. 3.

3.2 Mesh Sensitivity Analysis

In order to reduce the numerical error, a larger calculation domain is taken. The front part of the computational domain is the semicircle entrance with 30 times chord length and the back region of airfoil is a square with a length of 60 times the chord length. The computational domain is split in ICEM software based on structured quadrangles. Since the mesh density has great influence on the numerical results, the independence of different mesh numbers is verified. The coarser mesh can cause large errors, but too many grids will increase the computational expense. Only when the increase of the number of grids has little effect on the calculation results, then the numerical simulation results are meaningful. Four different mesh numbers are calculated. The same feature and also the same mesh structured are used in the four cases. Twenty layers of prismatic elements are set near the airfoil. The results are shown in Fig. 4. The mesh numbers of these are about 80000 in Mesh 3 and 120000 in Mesh 4. The result with 80000 or more elements has no significant difference of less than 0.1%. This means that the number of grid of 80000 is the optimum point for the calculations. Finally, we choose the grid setting of Mesh 3 with about 80000 cells for further study. Fig. 5 is the computational mesh domain of airfoil.

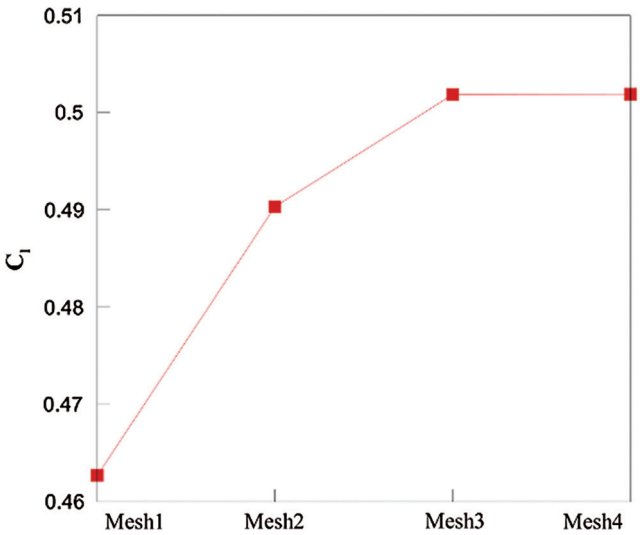

Figure 4: Mesh independence test results

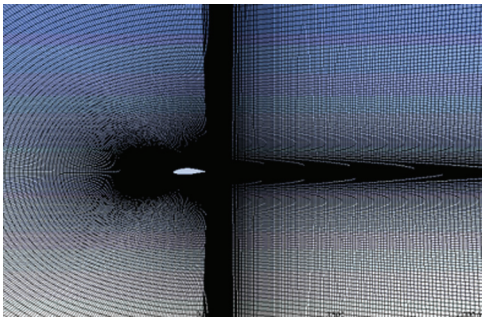

Figure 5: Computational mesh domain of airfoil

3.3 Boundary Conditions and Validation

The whole flow domain is set as incompressible, turbulent flow with steady calculation. The semicircle and upper and lower sides are set as the velocity inlet and the velocity is 56 m/s, Re = 7.7×10^6. Airfoil is set as no-slip wall condition The outlet boundary condition is set as free outflow and SST k-ω model is selected as the turbulence model. Initialize at the inlet. The finite volume method is used to discretize the differential equation, in which the convection term adopts the second-order upwind difference scheme and the diffusion term adopts the central difference scheme. SIMPLE method for coupling pressure and velocity; The discretized algebraic equation is solved iteratively by Gauss-Seidel. Residual convergence criterion is set to 10^{-4}. In order to verify the correctness of numerical simulation, compare the lift coefficient and drag coefficient with the UIUC (University of Illinois at Urbana-Champaign) Airfoil Coordinates Database. The airfoil to be compared is NACA 64A-010, Re = 10^6. The calculations are carried-out under the same physical parameters. Fig. 6 shows the comparison of lift coefficient and drag coefficient in numerical simulation and the UIUC Airfoil Coordinates Database.

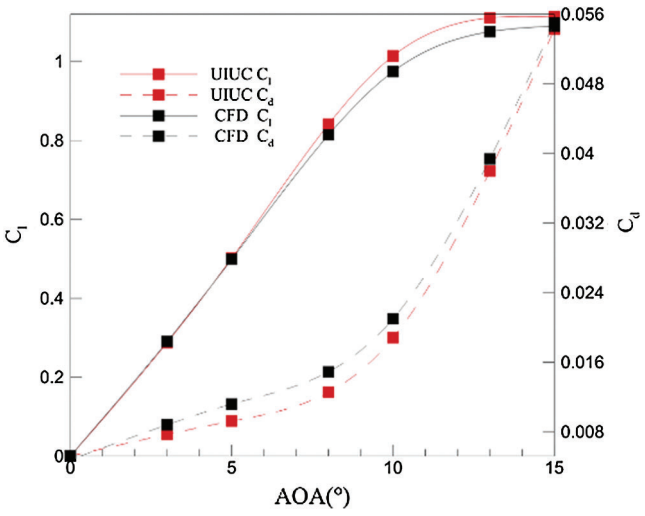

Figure 6: Comparison of CFD and UIUC

4 Results and Analysis

4.1 The Effect of Radius

Fig. 7 shows the relationship between the integral results and the airfoil radius at the angle of attack of 0°. Both of the integral result and the radius are dimensionless. The integral results are dimensionless by free

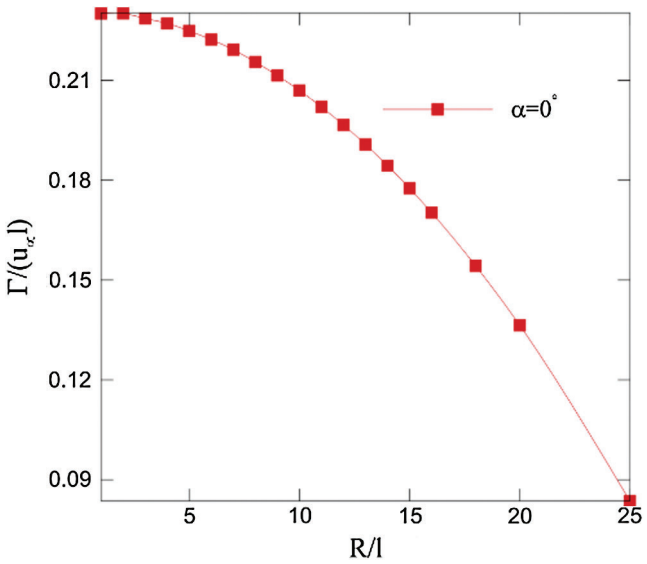

Figure 7: The relationship between integral value and radius

flow velocity u_∞ and chord length l. The radius is dimensionless by the chord length l. It can be seen from Fig. 4 that the integral value decreases gradually with the increase of the circle radius. When the radius is small, the integral value changes slightly with the radius. As the radius increases, the integral value decreases rapidly and change range is larger and larger. According to the theory of complete potential flow, the circulation value is constant with the difference of radius. The size of radius has no effect on the result. For incompressible flow, the influence area of turbulence on velocity is infinite. The calculation results show that the integral value gradually decreases with the increase of radius, which is because the fluid viscosity exists and circulation is dissipated in the flow process. According to the definition of circulation, it can be deduced that the integral result should tend to zero when the radius is large enough, which is confirmed by the results of calculation reasonably.

4.2 The Effect of Angle of Attack

The inflow angle of wind turbine blade is changing from root to tip, it is estimable to study the change of integral value with the angle of attack. Fig. 8 shows the trend of integral value with radius at different angles of attack and Fig. 9 shows the trend of integral value with angle of attack at different radii. The results show that the integral value changes with angle of attack and radius. With the increasing of angle of attack (AOA $\leq$ 12°), the integral value increases and the growth rate decreases gradually, which reaches a peak value at a certain angle of attack. Under different angles of attack, the integral value decreases with increasing of radius, and the trend of curve decrease tends to be consistent. In a certain range, according to the lift formula, the lift increases as the angle of attack increases. When the radius is small, the change range of integral value is small. The change range of integral value is greater when the angle of attack is the larger. The integral result is consistent with the circulation value derived from the lift formula.

According to the Kutta-Jukovsky theorem, for the lift of uniform constant velocity flow on an airfoil, the lift and lift coefficient mainly depend on the velocity circulation. Under the same operating conditions including angle of attack, airfoil and velocity, the circulation is a certain value. The result of integral calculation is equal to the value of circulation calculated by lift formula, but the result shows that the velocity vector integral in any path is not equal to the value of velocity circulation. Circulation can be inversely derived from the lift formula of the airfoil, which is used as a reference value. Tab. 1 shows the

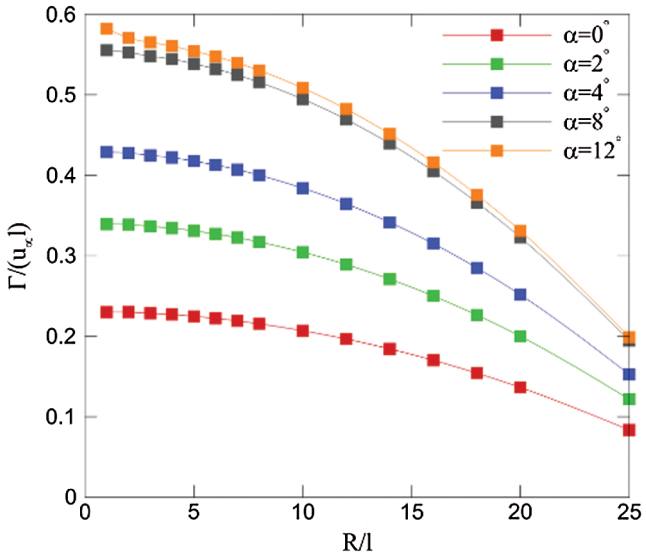

Figure 8: The variation of integral value with radius at different angles of attack

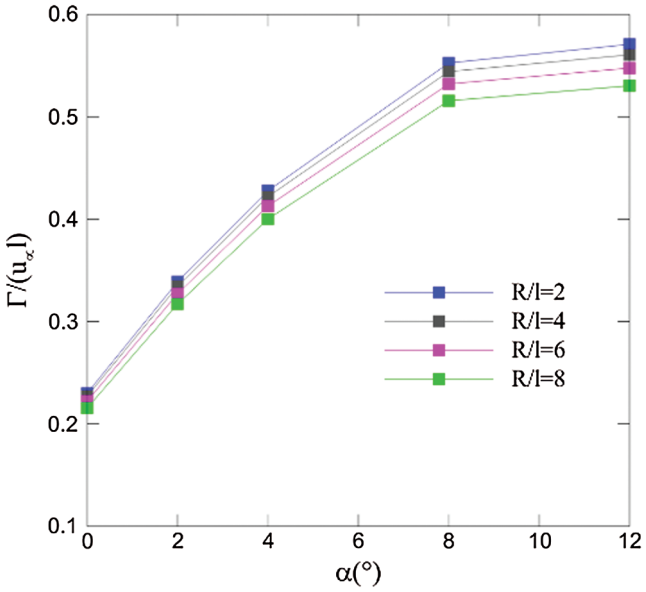

Figure 9: The variation of integral value with angle of attack at different radii

error between the integral value and the reference value of the airfoil at different angles of attack. The error is defined as:

$$error = \frac{\oint \boldsymbol{vds} - \dfrac{L}{\rho v}}{\dfrac{L}{\rho v}} = \frac{\oint \boldsymbol{vds} \cdot \rho v}{L} - 1 \tag{10}$$

It can be seen from the Tab. 1 that the error between the integral value and the reference value decreases under the same angle of attack. When reaching the minimum error, the error increases rapidly with the

Table 1: Error between integral value and circulation

$\alpha = 0°$	R/l	1	2	4	6	8	10	12
	Integral value (m^2/s)	25.77	25.77	25.44	24.89	24.14	23.18	22.02
	Error (%)	0.33	0.35	−0.94	−3.07	−6.00	−9.74	−19.59
$\alpha = 4°$	R/l	1	2	4	6	8	10	12
	Integral value (m^2/s)	48.01	47.91	47.26	46.78	46.23	44.82	40.83
	Error (%)	−1.83	−1.61	−0.23	1.95	4.95	8.77	13.40
$\alpha = 8°$	R/l	1	2	4	6	8	10	12
	Integral value (m^2/s)	62.20	61.89	60.95	59.60	57.75	55.40	52.57
	Error (%)	−1.43	−0.91	0.61	2.82	5.83	9.66	14.28
$\alpha = 12°$	R/l	1	2	4	6	8	10	12
	Integral value (m^2/s)	65.22	63.93	62.78	61.33	59.40	56.94	54.01
	Error (%)	−0.04	0.02	0.00	0.02	0.05	0.09	0.14

increase of the circle radius. The selection of the circle radius has a great influence on the integral value. There is a radius where the two values are equal. When the radius is 1–6 times chord length of the airfoil, it can guarantee that the error is within 5%. The optimal radius varies with different angles of attack.

4.3 Circulation Distribution of Blade of Wind Turbine

In order to study the circulation distribution of wind turbine blades, NREL 5 MW wind turbines is studied. According to the data provided by national renewable energy laboratory, a wind turbine model is established [18,19]. The three-dimensional model of blade is shown in Fig. 10. The impeller diameter is 126 m, the rated wind speed is 11.4 m/s, the cut in wind speed is 3 m/s, the cut out wind speed is 25 m/s, and the rated speed of the wind turbine is 12.1 r/min. The rotating field is a cylinder with a radius of 70 m. The height and width of stationary domain are 400 m and 600 m, respectively. The inlet and the outlet is 300 m and 500 m away from the rotating plane, respectively.

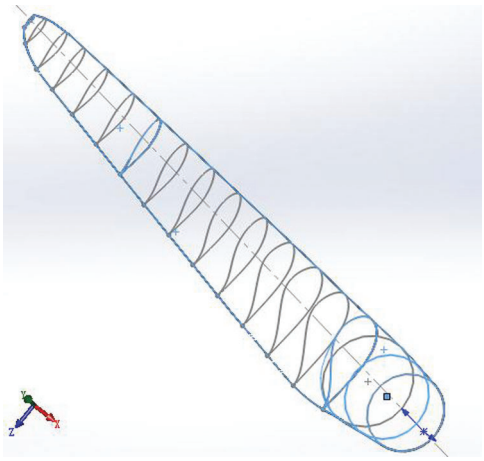

Figure 10: Three-dimensional model of blade

Because the blade structure of the wind turbine model is complex and the blade tail is too sharp, tetrahedral mesh is used for the simulation. The rotating domain is divided into relatively dense mesh. Ten layers of prismatic elements are divided near the blade. The thickness of the first layer of mesh is 0.01 m, with a growth rate of 1.2. In order to verify the mesh independence, by changing the maximum mesh size of the blade surface, the output power of wind turbine at the uniform rated wind speed (11.4 m/s) of 3.5 million, 4.65 million, 5.66 million and 6.82 million mesh cells are compared with the design value (5000 KW).The error of power given by the simulation and national renewable energy laboratory is controlled within 1% in order to ensure the correctness of the data, and 5.66 million unstructured mesh is selected for subsequent calculation. Tab. 2 shows the comparison of output power using different mesh numbers. Internal domain is the rotating domain, external is the static field. The sliding mesh method is used to simulate the rotation of the wind turbine [20,21]. Wind turbine blades and ground are set as wall and data is transferred through the interface interpolation. The inlet is set as velocity inlet and the velocity is 11.4 m/s. The bottom and blades are set as wall and the remaining faces of flow field are set as free flow. The SST k-ω model is selected as the turbulence model, which combines advantages of k-ω model calculation in the near wall area with the advantages of model far-field calculation. The model further modifies the turbulence viscosity and adds the orthogonal diffusion term, which can not only better predict the start of turbulence but also predict the flow separation effectively under negative pressure gradient. For the aerodynamic problems of wind turbines in this paper, the SST k-ω model has obvious advantages [22–24].

Table 2: Power comparison using different mesh resolutions

Mesh (million)	Simulation of power (KW)	Error with experimental value (%)
3.50	4630	7.4
4.65	4875	2.5
5.66	5044	0.88
6.82	5027	0.54

When calculating the integral value, the radius of the circle is 2 times the local chord length. Tab. 3 shows the average thrust and power of wind turbines under different rated wind speed and wind shear conditions, in which the wind shear exponent is 0.2. It can be seen from Tab. 2 that the thrust value of wind turbines decreases by 3.5% and the power decreases by 3.1% compared with the rated wind speed. Because the shear wind speed is distributed exponentially, the average wind speed of the shear incoming flow in the rotating surface of the wind wheel is less than the rated wind speed when the wind speed of the wheel hub is the same. Fig. 11 shows the circulation distribution at different blade length ratios. In this part, the blade is the same airfoil and aerodynamic center is in the same position. Because of the difference of absolute speed and inflow angle at different blade length ratios, circulation in each position is changing. The wind speed result in uneven blade aerodynamic performance deviates from the design point under the wind shear model. The circulation with different relative heights is lower than the circulation under the rated wind speed, so the average axial thrust and output power of the wind wheel under wind shear are lower than the rated wind speed. When the wind turbine works in the natural environment of the field, the complex working environment is affected by the changing incoming flow, which will affect the absorption of energy from the wind by the wind turbine.

Table 3: Thrust and power at different wind speeds

Variable	Thrust (KN)	Power (KW)
Rated wind speed	760.2	5044
Wind shear	733.4	4888

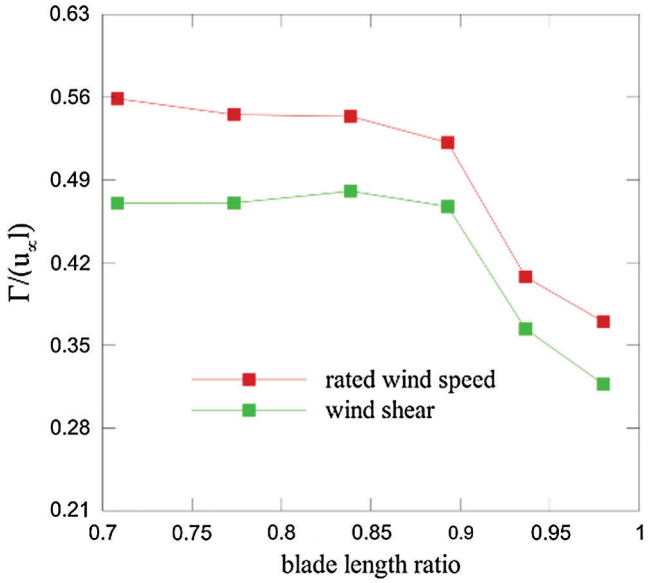

Figure 11: Circulation distribution of different blade length ratios at different wind speeds

5 Conclusion

In this paper, we tend to provide a specific method to integrate the circulation value around a two-dimensional airfoil and select the NACA64_A17 airfoil as a demonstration example to present how to find an optimal integral path for calculating the circulation. The blade circulation distribution of wind turbine is studied.

1. Because of the influence of viscosity, the integral value varies with the integral path. There is an optimal integral path where the value is the same as the circulation derived from the lift formula. When the integral radius is small, the change range of the integral value is relatively small, and the error increases rapidly with the increase of the radius.
2. The value of circulation and the optimal path of integration varies with the angle of attack. When the radius is 1–6 times chord length of the airfoil, it can guarantee that the error with the lift formula is within 5%.
3. The radial circulation distribution of the wind turbine blade is variable and the uneven wind speed will cause the aerodynamic characteristics of the blade to be biased to the design value, thus reducing the axial thrust and output power.

With the circulation distribution characteristics as the optimization design variable, changing blade parameters can optimize the blade design of the wind turbine, which is meaningful to the future design of the aerodynamically effective wind turbine blade based on the concept of flow control.

Acknowledgement: The authors like to express their thankfulness to the National supercomputer center in Jinan for providing computer facility during this work.

Funding Statement: This work was supported by the Shandong Provincial Natural Science Foundation, China (No. ZR2019QA018).

Conflicts of Interest: The authors declare that they have no conflicts of interest to report regarding the present study.

References

1. Paul, D. (2017). Global Wind Report Annual Market Update 2016.
2. Rasmussen, F., Hansen, M. H., Tomsen, K., Larsen, T. J., Bertagnolio, F. et al. (2003). Present status of aeroelasticity of wind turbines. *Wind Energy, 6(3),* 213–228. DOI 10.1002/we.98.
3. Benjanirat, S., Sankar, L., Xu, G. (2003). Evaluation of turbulence models for the prediction of wind turbine aerodynamics. *41st Aerospace Sciences Meeting and Exhibit, AIAA-2003-0517,* Reno, Nevada, USA. DOI 10.2514/6.2003-517.
4. Takizawa, K., Tezduyar, T. E., Otoguro, Y., Terahara, T., Kuraishi, T. et al. (2017). Turbocharger flow computations with the Space-Time Isogeometric Analysis (ST-IGA). *Computers & Fluids, 142,* 15–20. DOI 10.1016/j.compfluid.2016.02.021.
5. Zhang, Q. L. (2007). *Numerical study on three-dimensional aerodynamic performance of wind turbine blades (Ph.D. Thesis)*. Tsinghua University.
6. Tian, P., Huang, J., Shi, W., Zhou, L. (2019). Optimization of a centrifugal pump used as a turbine impeller by means of an orthogonal test approach. *Fluid Dynamics & Materials Processing, 15(2),* 139–151. DOI 10.32604/fdmp.2019.05216.
7. Yang, K., Wan, S. T., Kang, W. L. (2020). Pulsating wind speed model considering wind shear and tower shadow effect. *Journal of North China Electric Power University, 47(01),* 63–69.
8. Chen, Y., Duan, H., Yu, F., Zhao, X., Xu, H. et al. (2015). Parametric study of bubble kinematic behaviour in a centrifugal vacuum separator. *Fluid Dynamics & Materials Processing, 11(2),* 127–142.
9. Kriraa, M., Alami, M., Abouricha, M. (2014). Contribution to improving the performance of a wind turbine using natural convection. *Fluid Dynamics & Materials Processing, 10(4),* 443–464.
10. Frulla, G., Gili, P., Visone, M., D'Oriano, V., Lappa, M. (2015). A practical engineering approach to the design and manufacturing of a mini kW blade wind turbine: definition, optimization and CFD analysis. *FDMP-Fluid Dynamics & Materials Processing, 11(3),* 257–277.
11. Kim, Y., Lee, D. H., Kim, Y. (2002). Multidisciplinary design optimization of supersonic fighter wing using response surface methodology. *9th AIAA/ISSMO Symposium on Multidisciplinary Analysis and Optimization. AIAA 2002-5408*, Atlanta, Georgia, USA. DOI 10.2514/6.2002-5408.
12. Shi, G., Renaud, G., Yang, X. (2002). Integrated wing design with three disciplines. 9th AIAA/ISSMO Symposium on Multidisciplinary Analysis and Optimization. *AIAA 2002-5408, Atlanta*, Georgia, USA. DOI 10.2514/6.2002-5405.
13. Liem, R. P., Kenway, G. K. W., Martins, J. R. R. A. (2015). Multimission aircraft fuel-burn minimization via multipoint aerostructural optimization. *AIAA Journal, 53(1),* 104–122. DOI 10.2514/1.J052940.
14. Jiang, Y. V., Jia, H. G. (2017). Drag-reduction inverse design of wings based on lifting-line theory. *Optics and Precision Engineering, 25(5),* 1259–1265. DOI 10.3788/OPE.20172505.1259.
15. Qiao, C. L., Xu, H. Y., Ye, Z. Y. (2019). Circulation control on wind turbine airfoil with blunt trailing edge. *Acta Mechanica Sinica, 51(1),* 135–145.
16. Paterson, E. G., Baker, W. J., Kunz, R. F., Peltier, L. J. (2004). RANS and detached-eddy simulation of the NCCR airfoil. *2004 Users Group Conference (DOD_UGC'04)*. Wiliiamsburg, VA, USA. DOI 10.1109/dod_ugc.2004.38.
17. Song, Y. P., Yang, X. G., Li, Y. A. C. (2010). Numerical simulation of coanda effect in circulation control airfoil. *Journal of Engineering Thermophysics, 31(9),* 1475–1480.

18. Jonkman, J. M., Butterfield, S., Musial, W., Scott, G. (2009). *Definition of a 5-MW reference wind turbine for offshore system development (Technical Report)*. National Renewable Energy Laboratory (NREL). DOI 10.2172/947422.
19. Smith, K., Randall, G., Malcol, D. (2002). Evaluation of wind shear patterns at midwest wind energy facilities. *American Wind Energy Association Wind Power 2002 Conference,* Portland, Oregon, USA.
20. Guerri, O., Sakout, A., Bouhadef, K. (2007). Simulations of the fluid flow around a rotating vertical axis wind turbine. *Wind Engineering, 31(3),* 149–163. DOI 10.1260/030952407781998819.
21. Ren, Y., Liu, H. L., Shu, M. H., Wu, X. F., Wu, D. H. (2012). Improvement of SST k-ω turbulence model and numerical simulation in centrifugal pump. *Acta Agriculturae Mechanica Sinica, 43(11),* 123–128.
22. Yang, J. G., Wu, H. (2014). Explicit coupled solution of two-equation k-ω SST turbulence model and its application in turbomachine. *Acta Aeronautica Sinica, 35(1),* 116–124.
23. Qin, N., Vavalle, A., Le Moigne, A., Laban, M., Hackett, K. et al. (2004). Aerodynamic considerations of blended wing body aircraft. *Progress in Aerospace Sciences, 40(6),* 321–343. DOI 10.1016/j.paerosci.2004.08.001.
24. Abdelsalam, A. M., Hari Krishnan Kumar, S. S., Boopathi, K., Ramalingam, V. (2012). Numerical computations of wind turbine wakes using full rotor modeling. *IACSIT. Proceedings of 2012 2nd International Conference on Power and Energy Systems,* Pune, India. pp. 117–121.